Ariadne-Anne Tsambali¹ / Avraam A. Konstantinidis¹ / Elias C. Aifantis^{1,2,3,4}

Modelling double diffusion in soils and materials

- ¹ Aristotle University of Thessaloniki, Thessaloniki 54124, Greece, E-mail: akonsta@civil.auth.gr
- ² Michigan Technological University, Houghton, MI 49931, USA
- ³ ITMO University, St. Petersburg 197101, Russia
- ⁴ BUCEA, Beijing 100044, China

Abstract:

The double diffusivity model proposed earlier by Aifantis and co-workers was applied in this work for modelling the diffusion of metals in sandy aquifers, as well as chloride diffusion in concrete specimens. The theoretical predictions are in very good agreement with the measured concentrations in all cases, showing that the model is capable of dealing with a large variety of double diffusivity problems.

Keywords: diffusion in concrete, double diffusivity, metal transport

DOI: 10.1515/jmbm-2018-2003

1 Introduction

A double diffusivity model was initially proposed by Aifantis [1] and elaborated upon later by Aifantis and co-workers [2], [3], [4], [5], [6] to interpret diffusion processes in the presence of high-diffusivity paths. The double diffusivity model is a continuum model based on the assumption of two local non-equilibrium concentration fields obeying separate mass and momentum balance equations, with a linear constitutive equation for the mass exchange term between them. The aforementioned diffusion paths are the bulk or grain diffusion obeying Fick's second law where the logarithm of concentration c varies linearly with the square of the penetration depth x, and the surface diffusion taking place in internal surfaces, e.g. grain boundaries and triple junctions. Double diffusion manifests itself in semi-logarithmic plots of diffusive matter concentration vs. penetration depth through distinct regions of data forming lines with different slopes, from which the two diffusion coefficients are calculated. In certain cases, surface diffusion is several orders of magnitude larger than in the bulk. The double diffusion concept was extended to formulate a double diffusivity continuum model by Konstantinidis and Aifantis [6] and Kalampakas and Aifantis [7].

For media with different transport paths, Hughes and Sahimi [8] proposed a model for transport in heterogeneous solids and porous media which contain N distinct families of transport paths (with $N \ge 2$). The model is relevant to transport in metals, polycrystals, porous catalysts, coalbed methane reservoirs and geological systems with fractures and pores. Klein and Peszynska [9] used a double-diffusion model to simulate slightly compressible fluid flow in periodic porous media as a macro-model in place of the original highly heterogeneous micro-model. They presented an adaptive two-grid numerical finite-element discretisation of the double-diffusion system and performed a comparison between the micro- and macro-models.

For novel and nanostructured materials, Konstantinidis et al. [10] proposed a continuum double diffusivity model for the interpretation of experimental results on oxygen self-diffusion through grain boundaries of $YBa_2Cu_3O_{7-x}$ superconductors. The agreement between theory and experiment was very satisfactory. Recently, Aifantis [11], for the case of nanopolycrystals proposed that the grain boundaries may be viewed either as sources/sinks of "effective" mass and internal force or as a separate phase, interacting with the bulk phase that it surrounds, and supporting its own fields, balance laws and constitutive equations reflecting this interaction. In either view, a further common assumption introduced is that the constitutive interaction between bulk and "interface" phases enters in the form of higher order gradient terms, independently of the details of the underlying physical mechanisms that bring these terms about. The effectiveness of the approach is shown by considering certain benchmark problems for nanoelasticity, nanoplasticity and nanodiffusion for which standard continuum mechanics theory fails to model the observed behaviour.

Based on similar ideas, an extensive work can be found on the theory of molecular physiology and biophysics [12], [13], where one of the most dominant methods assumed for a large class of cellular processes is the reaction (or binding) diffusion kinetics, which are controlled by kinetic constants such as diffusion coefficients and on/off binding rate constants.

In the next section the methodology of the double-diffusivity formulation is described, and in Section 3 its application in various cases, while further developments on the application of double-diffusivity models in various processes and materials can be found in [14], [15], [16], [17], [18], [19], [20], [21].

2 Methodology

The double diffusivity model [6] assumes two diffusion paths, namely the lattice and the dislocation or grain boundary one, designated by the indices "1" and "2", respectively, which are viewed as continuously distributed in space and time.

Let c_1 and c_2 denote the concentrations of the diffusing species in paths "1" and "2", and j_1 and j_2 their diffusion fluxes. Assuming that Fick's law holds for each path separately, and that mass exchange takes place between the two types of diffusion paths, then the equation of mass concentration $\partial c_a/\partial t + divj_a = q_a$, leads to the following constitutive equations

$$\frac{\partial c_1}{\partial t} = D_1 \nabla^2 c_1 - \kappa_1 c_1 + \kappa_2 c_2, \quad \frac{\partial c_2}{\partial t} = D_2 \nabla^2 c_2 + \kappa_1 c_1 - \kappa_2 c_2, \tag{1}$$

where D_1 , D_2 are the diffusion coefficients for each path separately and κ_1 , κ_2 are the "reaction" constants designating the interaction between paths.

We consider Eqs. (1) as the fundamental differential equations which describe simultaneous diffusion through high-diffusivity and regular diffusion paths, or simultaneous diffusion of vacancies. The diffusing species concentrations coming from Eqs. (1) for the case of a one-dimensional semi-infinite medium extending in the x direction are given by

$$c_1(x,\,t) = e^{-\kappa_1 t} h_1(x,\,D_1 t) + \frac{\sqrt{\kappa_2} e^{\lambda t}}{D_1 - D_2} \int\limits_{D_2 t}^{D_1 t} e^{-\mu \xi} \left\{ \sqrt{\kappa_1 \frac{\xi - D_2 t}{D_1 t - \xi}} I_1(\eta) h_1(x,\,\xi) + \sqrt{\kappa_2} I_0(\eta) h_2(x,\,\xi) \right\} d\xi, \tag{2}$$

$$c_2(x,\,t) = e^{-\kappa_2 t} h_2(x,\,D_2 t) + \frac{\sqrt{\kappa_1} e^{\lambda t}}{D_1 - D_2} \int\limits_{D_2 t}^{D_1 t} e^{-\mu \xi} \left\{ \sqrt{\kappa_2 \frac{D_1 t - \xi}{\xi - D_2 t}} I_1(\eta) h_2(x,\,\xi) + \sqrt{\kappa_1} I_0(\eta) h_1(x,\,\xi) \right\} d\xi, \tag{3}$$

where $I_{0,1}$ denote modified Bessel functions and the remaining quantities (λ, μ, η) are given by $\lambda = (\kappa_1 D_2 - \kappa_2 D_1)/(D_1 - D_2)$, $\mu = (\kappa_1 - \kappa_2)/(D_1 - D_2)$, $\eta = 2\sqrt{\kappa_1 \kappa_2(D_1 t - \xi)(\xi - D_2 t)}/(D_1 - D_2)$. The functions $h_1(x, t)$ and $h_2(x, t)$, are the unique solutions of the "classical" diffusion equation $\partial h/\partial t = \nabla^2 h$.

Furthermore, we suppose that for a semi-infinite medium with finite source of diffusing substance placed at the origin ("thin film" initial condition), the functions h_1 , h_2 have the following form

$$h_1(x, t) = \frac{M_1}{2\sqrt{\pi t}}e^{-x^2/4t}, h_2(x, t) = \frac{M_2}{2\sqrt{\pi t}}e^{-x^2/4t},$$
 (4)

where M_1 , M_2 denote the initial amounts of diffusing substances in the form of a thin film in contact with the specimen's surface occupied simultaneously by the two types of diffusion paths. Then total concentration of the diffusing species in both paths is calculated by addition of Eqs. (2) and (3), to obtain

$$c(x, t) = c_1(x, t) + c_2(x, t)$$
(5)

The formulation presented in this section is applied in various diffusion problems and the theoretical predictions are compared with simulation results as well as experimental measurements.

3 Applications and results

3.1 Reactive transport of metals in sandy aquifers

Organic carbon introduction in soil to initiate remedial measures, nitrate infiltration due to agricultural practices or sulfate intrusion owing to industrial usage can influence the redox conditions and pH, thus affecting the

Automatically generated rough PDF by ProofCheck from River Valley Technologies Ltd

mobility of heavy metals in soil and groundwater. Satyawall et al. [22] reported the fate of Zn and Cd in sandy aquifers under a variety of plausible in-situ redox conditions that were induced by introduction of carbon and various electron acceptors in four column experiments. Up to 100% Zn and Cd removal (from the liquid phase) was observed in all four columns, however the mechanisms were different. Metal removal in column K1 (containing sulfate), was attributed to biological sulfate reduction and subsequent metal precipitation (as sulfides). In the presence of both nitrate and sulfate (K2), the former dominated the process, precipitating the heavy metals as hydroxides and/or carbonates. In the presence of sulfate, nitrate and supplemental iron [Fe(OH)₃] (K3), metal removal was also due to precipitation as hydroxides and/or carbonates. In abiotic column, K4, [with supplemental iron (Fe(OH)₃), but no nitrate], cation exchange with soil led to metal removal.

3.1.1 Zn and Cd removal profile with pH variation in K4 after 61 days

The simulation results [22] for this case, shown in Figure 1A, were modelled through Eq. (5), with the various model parameters given in Table 1, while the comparison with the theoretical predictions is shown in Figure 1B.

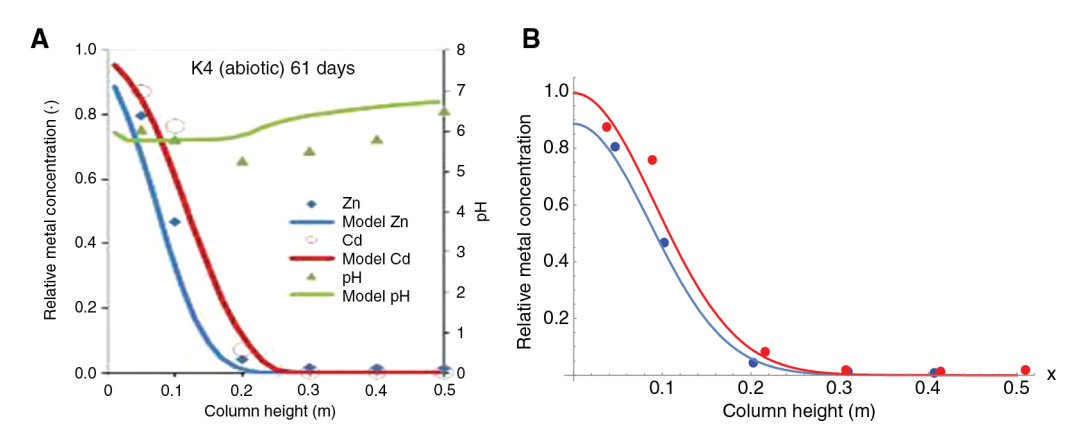


Figure 1: (A) Zn and Cd removal profile with pH variation in K4 after 61 days. (B) Comparison between theoretical predictions and simulation results.

Table 1: Parameter values for Zn and Cd removal profile with pH variation in K4 after 61 days.

| | κ_1 (s ⁻¹) | κ_2 (s ⁻¹) | <i>t</i> (s) | D_1 (m ² /s) | D_2 (m ² /s) | M_1 | M_2 |
|----|-------------------------------|-------------------------------|--------------|---------------------------|---------------------------|-------|-------|
| Zn | 9 10-9 | $12 \ 10^{-13}$ | 5,270,400 | $7\ 10^{-10}$ | $4\ 10^{-1}$ | 0.2 | 0.12 |
| Cd | $9\ 10^{-9}$ | $12 \ 10^{-13}$ | 5,270,400 | $8 \ 10^{-10}$ | $4 \ 10^{-1}$ | 0.24 | 0.12 |

3.1.2 Zn removal profile after 100 d in case of carbon/sulfate/nitrate intrusion

The removal of heavy metals in case of carbon intrusion after application of 10 mg/l (0.17 mm) acetate [in the presence of 60 mg/l (0.62 mm) sulfate] was much faster (due to sulfate reduction and metal precipitation as sulfides). The simulation results [22] in this case are shown in Figure 2A, and the comparison between them and the theoretical predictions of Eq. (5), where the various model parameters are given in Table 2, is shown in Figure 2B. Analogous comparisons in the cases of sulfate and nitrate intrusion are provided in Table 3 and Figure 3, and Table 4 and Figure 4, respectively.

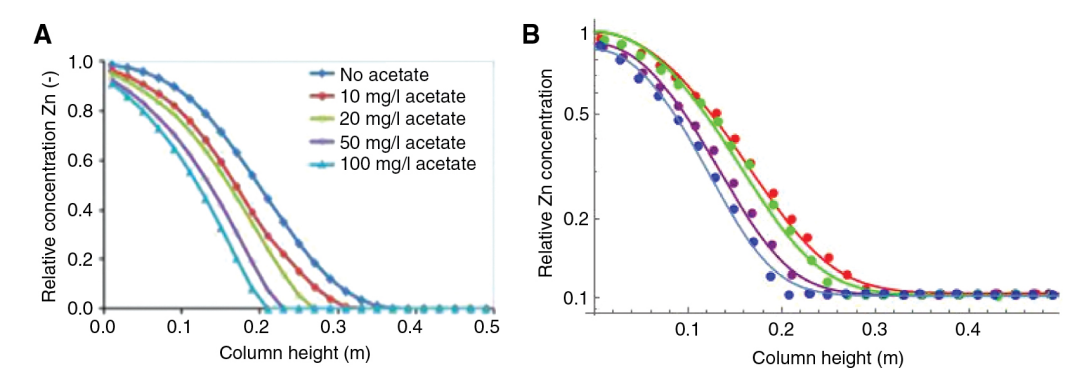


Figure 2: (A) Zn removal profile after 100 days in case of carbon source intrusion (bioremediation condition). Assumed: 60 mg/l sulfate. (B) Comparison between theoretical predictions and simulation results [22].

Table 2: Parameter values for Zn removal profile in case of carbon intrusion after 100 days.

| Accecate | κ_1 (s ⁻¹) | κ_2 (s ⁻¹) | t (s) | D_1 (m ² /s) | D_2 (m ² /s) | M_1 | M_2 |
|----------|-------------------------------|-------------------------------|-----------|---------------------------|---------------------------|-------|-------|
| 0 mg/l | 9 10-9 | $12\ 10^{-9}$ | 8,640,000 | $10 \ 10^{-10}$ | $4\ 10^{-1}$ | 0.36 | 0.12 |
| 10 mg/l | $9\ 10^{-9}$ | $12\ 10^{-9}$ | 8,640,000 | $9\ 10^{-10}$ | $4 \ 10^{-1}$ | 0.32 | 0.12 |
| 20 mg/l | $8 \ 10^{-9}$ | $12 \ 10^{-9}$ | 8,640,000 | $6\ 10^{-10}$ | $4 \ 10^{-1}$ | 0.25 | 0.12 |
| 50 mg/l | 510^{-9} | $12\ 10^{-9}$ | 8,640,000 | $5 \ 10^{-10}$ | $4 \ 10^{-1}$ | 0.22 | 0.12 |

Table 3: Parameter values for Zn removal profile in case of sulfate intrusion after 100 days.

| Sulfate | $\kappa_1 (s^{-1})$ | κ_2 (s ⁻¹) | t (s) | D_1 (m ² /s) | D_2 (m ² /s) | M_1 | M_2 |
|----------|----------------------|-------------------------------|-----------|---------------------------|---------------------------|-------|-------|
| 0 mg/l | $8 \ 10^{-9}$ | $12\ 10^{-9}$ | 8,640,000 | $10 \ 10^{-10}$ | $4 \ 10^{-1}$ | 0.35 | 0.12 |
| 10 mg/l | $8 \ 10^{-9}$ | $12\ 10^{-9}$ | 8,640,000 | $8\ 10^{-10}$ | $4\ 10^{-1}$ | 0.3 | 0.12 |
| 20 mg/l | $9\ 10^{-9}$ | $12\ 10^{-9}$ | 8,640,000 | $6\ 10^{-10}$ | $4\ 10^{-1}$ | 0.26 | 0.12 |
| 100 mg/l | $5 \ 10^{-9}$ | $12 \ 10^{-9}$ | 8,640,000 | $4.5 \ 10^{-10}$ | $4 \ 10^{-1}$ | 0.22 | 0.12 |

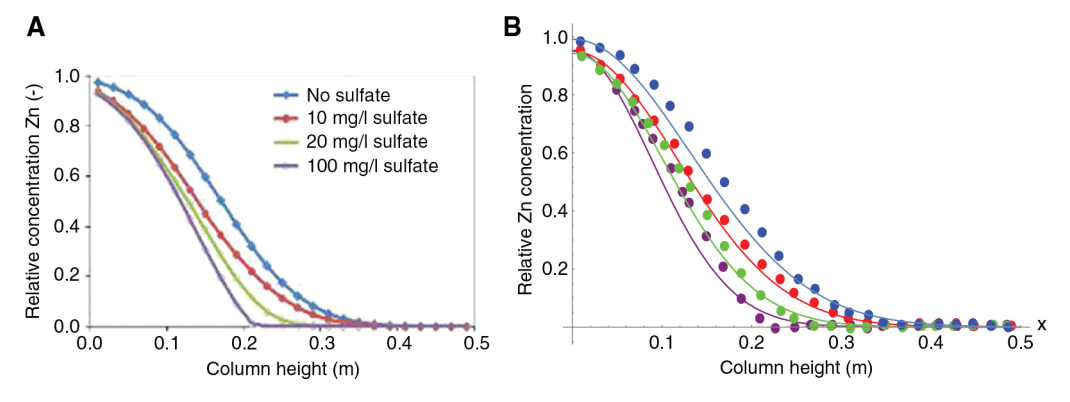


Figure 3: (A) Zn removal profile after 100 days in case of sulfate intrusion. (B) Comparison between theoretical predictions and simulation results [22].

Table 4: Parameter values for Zn removal profile in case of nitrate intrusion after 100 days.

| Nitrate | κ_1 (s ⁻¹) | κ_2 (s ⁻¹) | t (s) | D_1 (m ² /s) | D_2 (m ² /s) | M_1 | M_2 |
|----------|-------------------------------|-------------------------------|-----------|---------------------------|---------------------------|-------|-------|
| 0 mg/l | $10 \ 10^{-9}$ | $12\ 10^{-9}$ | 8,640,000 | $9\ 10^{-10}$ | $4 \ 10^{-1}$ | 0.32 | 0.12 |
| 10 mg/l | $9 \ 10^{-9}$ | $12\ 10^{-9}$ | 8,640,000 | $9\ 10^{-10}$ | $4 \ 10^{-1}$ | 0.32 | 0.12 |
| 20 mg/l | $10\ 10^{-9}$ | $12\ 10^{-9}$ | 8,640,000 | $9\ 10^{-10}$ | $4\ 10^{-1}$ | 0.26 | 0.12 |
| 100 mg/l | $8 \ 10^{-9}$ | $12\ 10^{-9}$ | 8,640,000 | $8\ 10^{-10}$ | $4\ 10^{-1}$ | 0.24 | 0.12 |

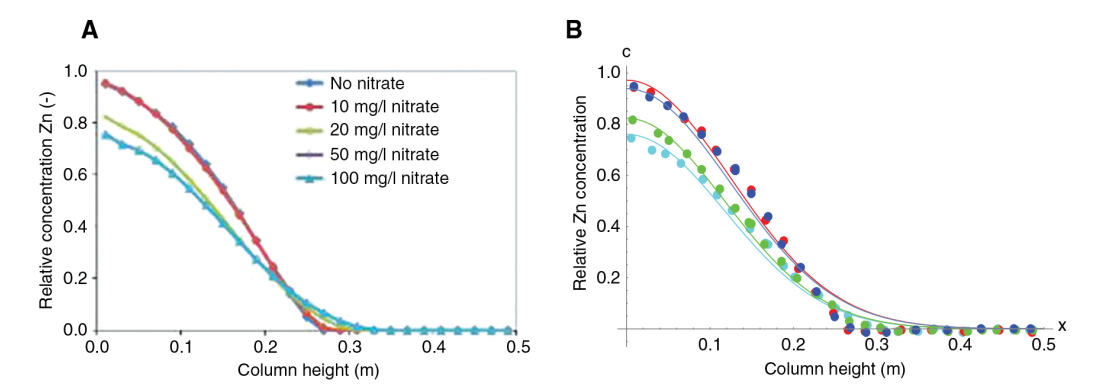


Figure 4: (A) Zn removal profile after 100 days in case of nitrate intrusion. (B) Comparison between theoretical predictions and simulation results [22].

3.2 Chloride diffusion in concrete containing nano-TiO,

The advantage of concrete containing nano- TiO_2 in resisting the coupled effects of chloride diffusion and scouring with respect to pure concrete was studied in the work of Li et al. [23]. Because of the movement in exposed concrete surface induced by scouring and the deterioration in concrete microstructure caused by chloride salt accumulation, an increasing mutual accelerative effect between the chloride diffusion and the scouring abrasion was experimentally observed, which agreed with the theoretical simulation results. Benefited from the improvement in microstructure and porosity compared with the pure concrete, concrete samples containing 1% nano- TiO_2 in the weight of cement showed a better impermeability as well as abradability. Correspondingly, a better performance in resisting the coupled effects of chloride diffusion and scouring was found for the concrete containing nano- TiO_2 compared to the pure concrete, and this advantage increased upon time.

Again, Eq. (5) was used for modeling the chloride concentrations in pure concrete shown in Figure 5A [23], as well as concrete containing nano- TiO_2 shown in Figure 6A [23], with the respective model parameters given in Table 5 and Table 6, respectively.

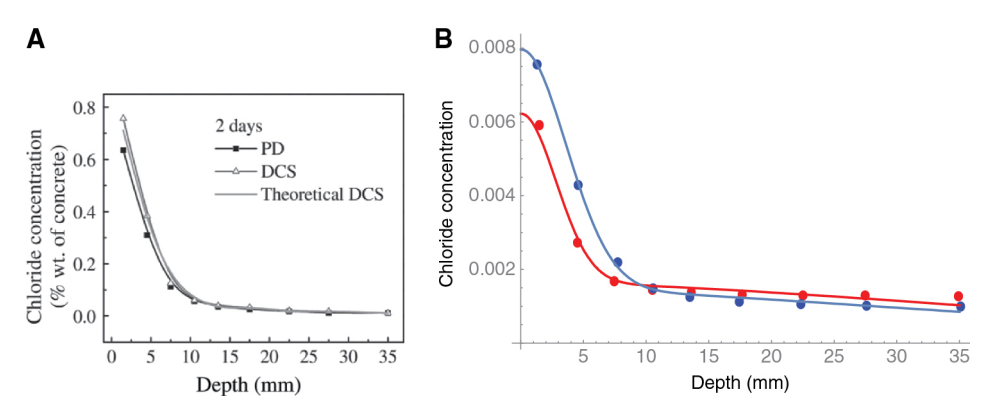


Figure 5: (A) Chloride concentrations of pure concrete as a function of depth under pure diffusion (PD) and diffusion coupled scouring (DCS). (B) Comparison between theoretical predictions and simulation results [23].

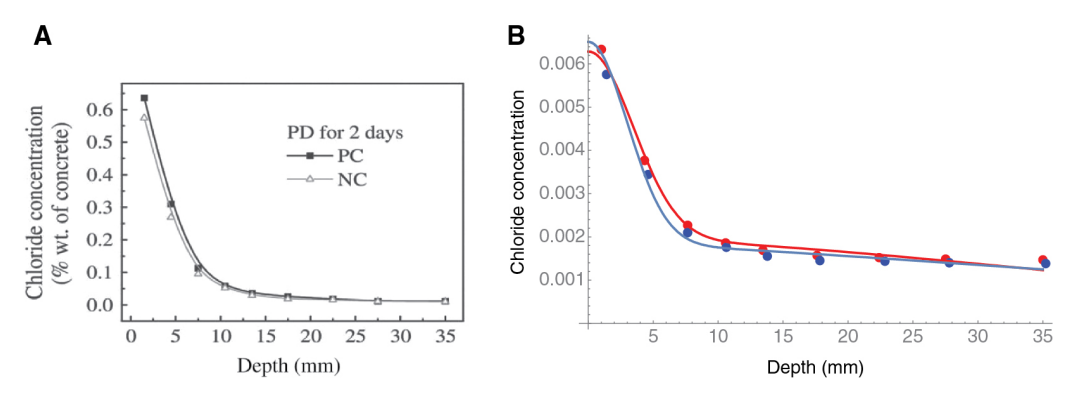


Figure 6: (A) Chloride concentrations of pure concrete as a function of depth in powdered concrete (PC) and nano-TiO₂ on cement (NC). (B) Comparison between theoretical predictions and simulation results [23].

Table 5: Parameter values for chloride concentrations of pure concrete under PD after 2 days.

| 2 days | κ_1 (d ⁻¹) | $\kappa_2 (\mathrm{d}^{-1})$ | t (d) | D_1 (mm ² /d) | D_2 (mm ² /d) | M_1 | M_2 |
|--------|-------------------------------|------------------------------|-------|----------------------------|----------------------------|-------|-------|
| Pd | $8 \ 10^{-6}$ | $2\ 10^{-1}$ | 2 | $4\ 10^2$ | 1.935 | 0.138 | 0.047 |
| DCS | $8 \ 10^{-6}$ | $2\ 10^{-1}$ | 2 | $4 \ 10^2$ | 3.2267 | 0.101 | 0.086 |

Table 6: Parameter values for chloride concentrations of pure concrete under PD after 2 days.

| 2 days | κ_1 (d ⁻¹) | $\kappa_2 (\mathrm{d}^{-1})$ | t (d) | D_1 (mm ² /d) | D_2 (mm ² /d) | M_1 | M_2 |
|--------|-------------------------------|------------------------------|-------|----------------------------|----------------------------|-------|-------|
| PC | 8 10 ⁻⁶ | $2 \cdot 10^{-1}$ | 2 | $4 \cdot 10^2$ | 2.935 | 0.166 | 0.055 |
| NC | $8 \ 10^{-6}$ | $2 \ 10^{-1}$ | 2 | $7.6 \ 10^2$ | 2.2267 | 0.128 | 0.115 |

3.3 Probabilistic considerations on the effect of specimen size on the critical chloride content in reinforced concrete

The durability of reinforced concrete structures is impacted by the chloride penetration and susceptibility of the reinforcement to chloride-induced corrosion when larger metal areas are exposed to air. Once the chloride content at the reinforcement reaches a threshold value and enough oxygen and moisture are present, the reinforcement corrosion will be initiated. Chloride penetration may result in the accumulation of chloride content at reinforcement to such a level that the high alkaline environment is destroyed and then the passivated film on the steel surface is disrupted. Corrosion products then accumulate in the concrete-steel interface transition zone cause crack initiation and propagation. The chloride concentration increases with increasing the area of exposed metal surface. The entire chloride-induced reinforcement corrosion process of reinforced concrete structures was modeled in [24] with a probabilistic model, which predicts the critical chloride content ($C_{\rm crit}$) for reinforcement corrosion as a function of specimen size.

The simulation results [24] for this case, shown in Figure 7A, were modelled through Eq. (5), with the various model parameters given in Table 7, while the comparison with the theoretical predictions is shown in Figure 7B.

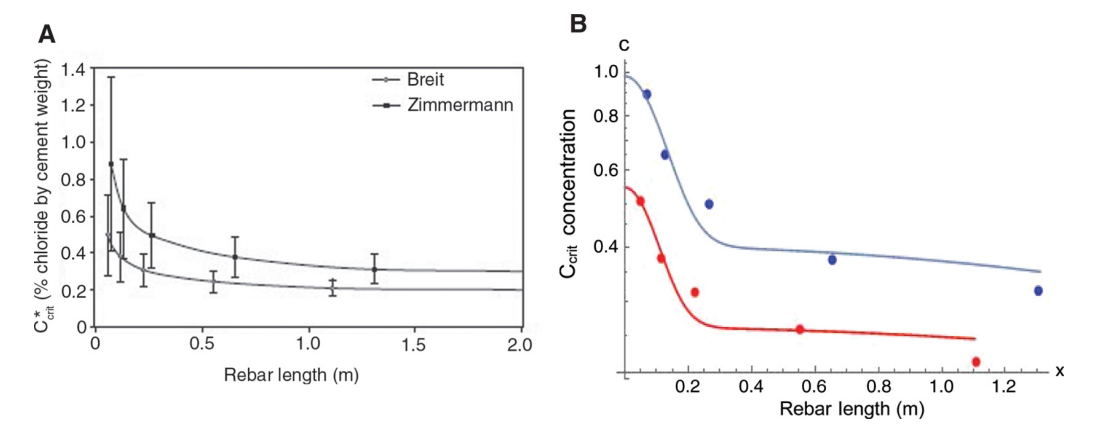


Figure 7: (A) Predicted mean value of C_{crit} as a function of specimen size which is expressed in rebar length [24]. (B) Comparison between theoretical predictions and simulation results [24].

Table 7: Parameter values for C_{crit.} chloride concentrations of reinforced concrete.

| | $\kappa_1 \; (s^{-1})$ | κ_2 (s ⁻¹) | t (s) | D_1 (m ² /s) | D_2 (m ² /s) | M_1 | M_2 |
|---------------------|--|----------------------------------|--------------|---|-----------------------------------|----------------|----------------|
| Breit Zimmermann | 16 10 ⁻⁹ 16 10 ⁻⁹ | $12 \ 10^{-13} $ $12 \ 10^{-13}$ | 3228 3228 | 1592.69 10 ⁻⁶ 892.69 10 ⁻⁶ | $1.26 \ 10^{-6}$ $2.06 \ 10^{-6}$ | 1.330 1.290 | 0.024 0.104 |

Automatically generated rough PDF by *ProofCheck* from River Valley Technologies Ltd

4 Discussion

A double diffusivity model by Aifantis and co-workers which was applied earlier for modelling diffusion problems in novel and nanostructured materials as well as nanopolycrystals, was applied herein for modelling diffusion of metals in sandy aquifers, as well as chloride diffusion in concrete specimens, providing predictions in very good agreement with experiments, showing that the model is capable of dealing with a large variety of double diffusivity problems.

Acknowledgements

The second and third author acknowledge the support of the Ministry of Education and Science of Russian Federation under Mega Grant No. 14.Z50.31.0039 to Togliatti State University.

References

- [1] Aifantis EC. J. Appl. Phys. 1979, 50, 3.
- [2] Hill JM, Aifantis EC. Quart. J. Mech. Appl. Math. 1980, 33, 1.
- [3] Hill JM, Aifantis EC. Quart. J. Mech. Appl. Math. 1980, 33, 23.
- [4] Moutsolpoulos KN, Eleftheriadis IE, Aifantis EC. Mech. Res. Commun. 1996, 23, 577–582.
- [5] Konstantinidis DA, Eleftheriadis IE, Aifantis EC. Scripta Mater. 1998, 38, 573-580.
- [6] Konstantinidis DA, Aifantis EC. Scripta Mater. 1999, 40, 1235–1241.
- [7] Kalampakas A, Aifantis EC. Mech. Res. Commun. 2012, 43, 101–104.
- [8] Hughes BD, Sahimi M. Phys. Rev. E 1993, 48, 2776.
- [9] Klein V, Peszynska M. J. Appl. Math. 2012, 938727, doi:10.1155/2012/938727.
- [10] Konstantinidis D, Eleftheriadis I, Aifantis EC. J. Mater. Process. Technol. 2001, 108, 185–187.
- [11] Aifantis EC. Metall. Mater. Trans. A 2011, 42.
- [12] Kang M, Kenworthy AK. Biophys. J.: Biophys. Lett. 2008, 95, L13-L15.
- [13] Kang M, Day CA, DiBenedetto E, Kenworthy AK. Biophys. J. 2010, 99, 2737–2747.
- [14] Lee Al, Hill JM. J. Math. Anal. Appl. 1982, 89, 530-557.
- [15] Jódar L, Goberna D. Comput. Math. Appl. 1996, 31, 17–24.
- [16] Angelakis A, Kadir T, Rolston D. Water Resour. Res. 1993, 29, 945–956.
- [17] Chernukha OYu, Dmytruk VA. J. Math. Sci. 2014, 201, 245–261.
- [18] Chaplya Y, Chernukha O, Dmytruk V. Appl. Math. Model. 2013, 37, 6191–6211.
- [19] Poznanski RR. J. Integr. Neurosci. 2010, 9, 283–297.
- [20] Camacho J, Jódar L, Navarro E. Math. Comput. Model. 1998, 28, 65–76.
- [21] Tully B, Ventikos Y. J. Fluid Mech. 2011, 667, 188–215.
- [22] Satyawall Y, Seuntjens P, Van Roy S, Joris I, Vangeel S, Dejonghe W, Vanbroekhoven K. J. Contam. Hydrol. 2011, 123, 83–93.
- [23] Li H, Xiao H, Guan X, Wang Z, Lei Yu. Compos. B 2014, 56, 698-704.
- [24] Angst U, Rønnquist A, Elsener B, Larsen CK, Vennesland O. Corros. Sci. 2011, 53, 177–187.